Supplement of Weather Clim. Dynam., 1, 519–539, 2020
https://doi.org/10.5194/wcd-1-519-2020-supplement

Supplement of

Dominant patterns of interaction between the tropics and mid-latitudes in boreal summer: causal relationships and the role of timescales

Giorgia Di Capua et al.

Correspondence to: Giorgia Di Capua (dicapua@pik-potsdam.de)

SI Text S1.

Using OLR composites, we explicitly show that the temporal evolution of the SAM convective activity at weekly time scales resembles the evolution of the Boreal Summer Intraseasonal Oscillation (BSISO) (Goswami and Ajaya Mohan, 2001; Saha et al., 2012) (see Fig. S2 in the Supplementary Material). The OLR pattern depicted by the first MCA mode represents phase 4-5 of the BSISO evolution (Fig. S2). The BSISO is characterized by a rainfall band tilted from northeast to southwest propagating from the tropical Indian Ocean toward Southeast Asia with a period of about one to two months. To further explore this hypothesis, we present a Wheeler-Hendon diagram using the BSISO index as defined by Kikuchi (2010) and plot (using different colours) BSISO phases that correspond to different lags (as defined considering the MCA mode 1 pattern for OLR as lag 0, see Fig. S2). The results show that each lag tends to cluster consistently around the corresponding BSISO phase (see Fig. S3a in the Supplementary Material). This suggests that the BSISO may exert a large-scale tropical control on mid-latitude anomalies, using variations in SAM rainfall as a pathway. When the same approach is applied to the WNPSM pattern, no consistent behaviour can be identified (Fig. S3b).

Parameters used for PCMCI (see https://jakobrunge.github.io/tigramite/#tigramite.pcmci.PCMCI for further explanation):

For causal map (Figs. 3,4,5 in the main text):

Pc_alpha = 0.2

Alpha level to print results= 0.05

Weekly: tau max = -2, tau min = 0

4-weekly: tau_max =1, tau min = 0

selected_links=None

max_conds_dim=None

max_combinations=1

max_conds_py=None,

max_conds_px=None

For CEN (Fig. 6 in the main text):

Pc_alpha = None (PCMCI default)

Alpha level to print results= 0.05

Weekly: tau max = -2, tau min = 0

4-weekly: tau_max =1, tau min = 0

selected_links=None

max_conds_dim=None

max_combinations=1

max_conds_py=None,

max_conds_px=None

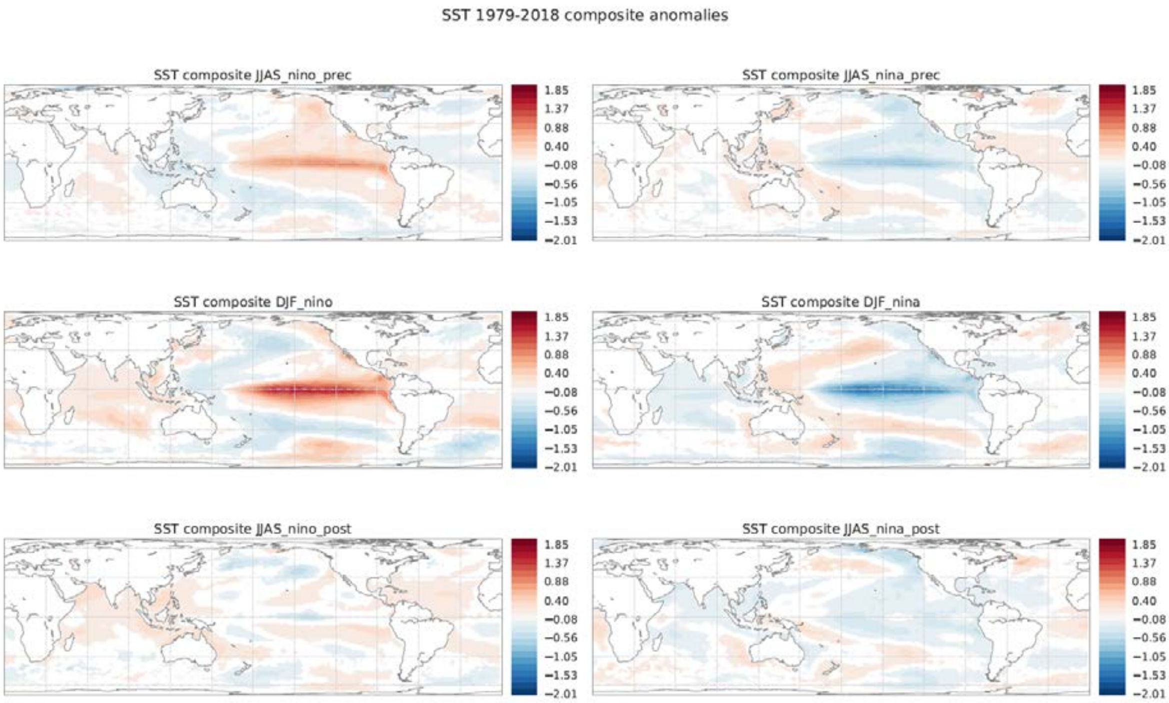

Figure S1. Composites of seasonal averaged SST anomalies for summer JJAS preceding El Niño, winter (DJF) with El Niño peak an summers following El Niño (left column). Right column: Same as left column but for La Niña years.

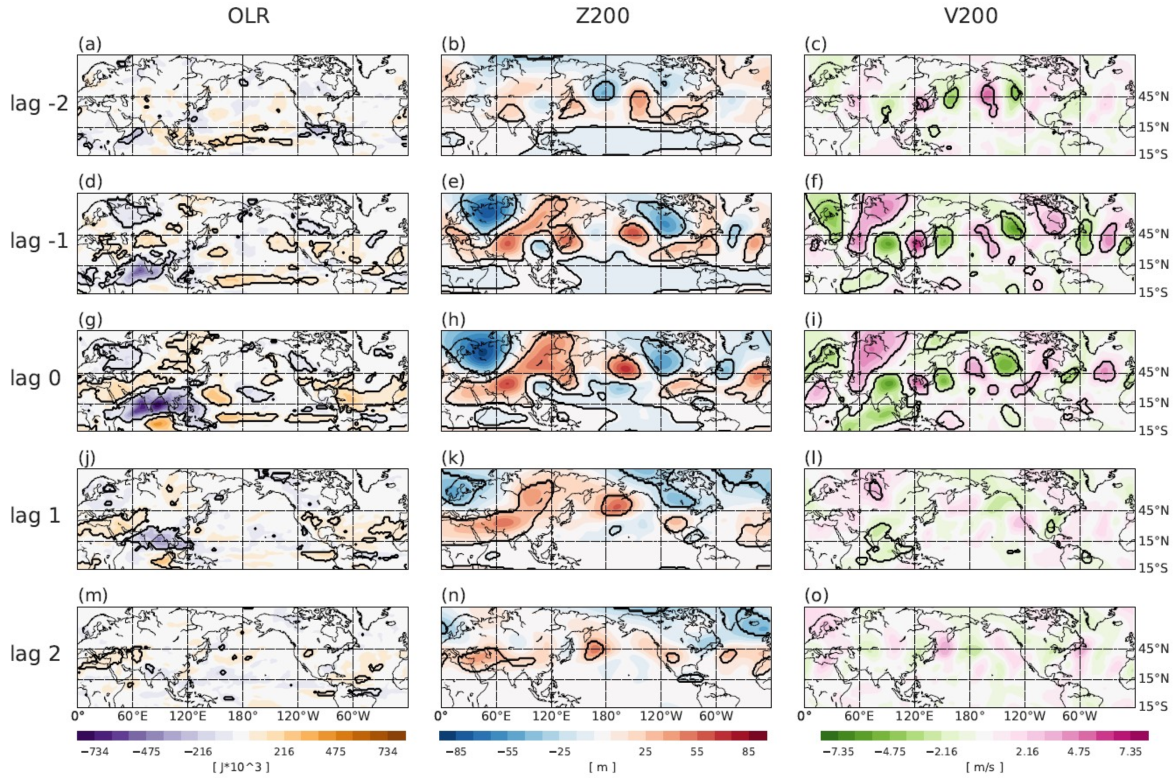

Figure S2. Time evolution of weekly tropical and mid-latitude anomalies. Composites of weekly OLR (left column), Z200 (central column) and V200 (right column) fields are calculated for weeks with high MCA mode 1 OLR scores (M1OLR) and M1OLR > $M1OLR_{std}$ minus weeks with low M1OLR (M1OLR < $M1OLR_{std}$). Here, lag 0 refers to the weeks where the M1OLR anomalies larger or smaller than $M1OLR_{std}$ are identified. Lags -1 and -2 are defined as 1 and 2 weeks prior lag 0, while lags +1 and +2 are defined as 1 and 2 weeks following lag 0.

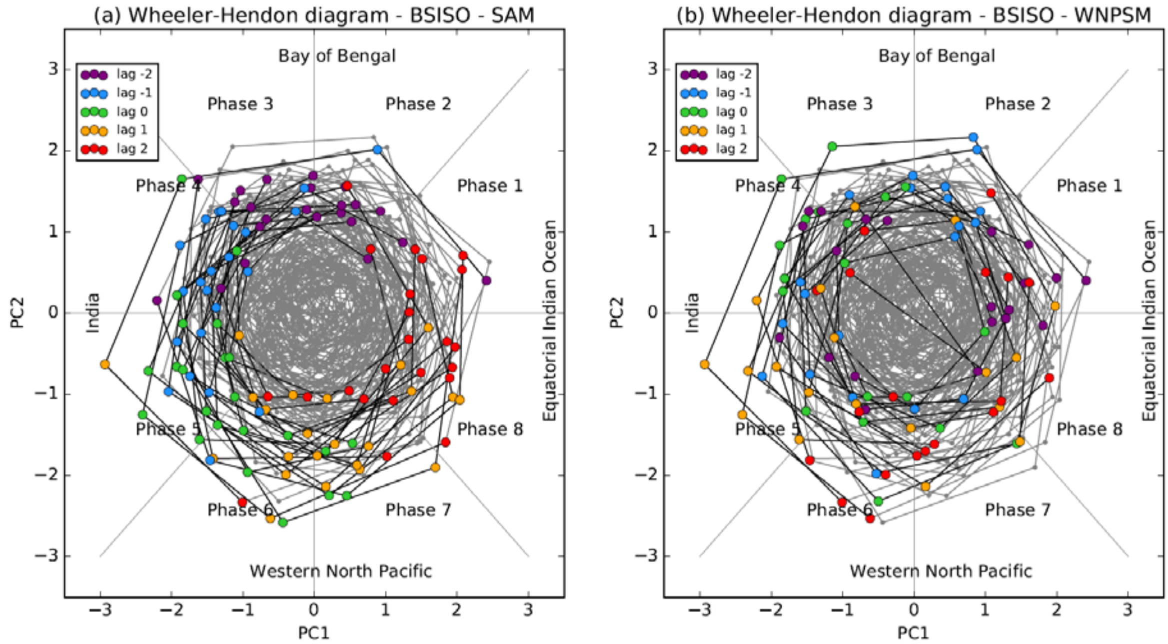

Figure S3. BSISO time evolution. BSISO data from Kikuchi et al. (2010) weekly averaged. The colour of each point in the Wheeler-Hendon diagram represents different lags defined as in Fig. S2. For simplicity, overlapping events are shown only once (only the event that stars first in time is shown). See SI text.

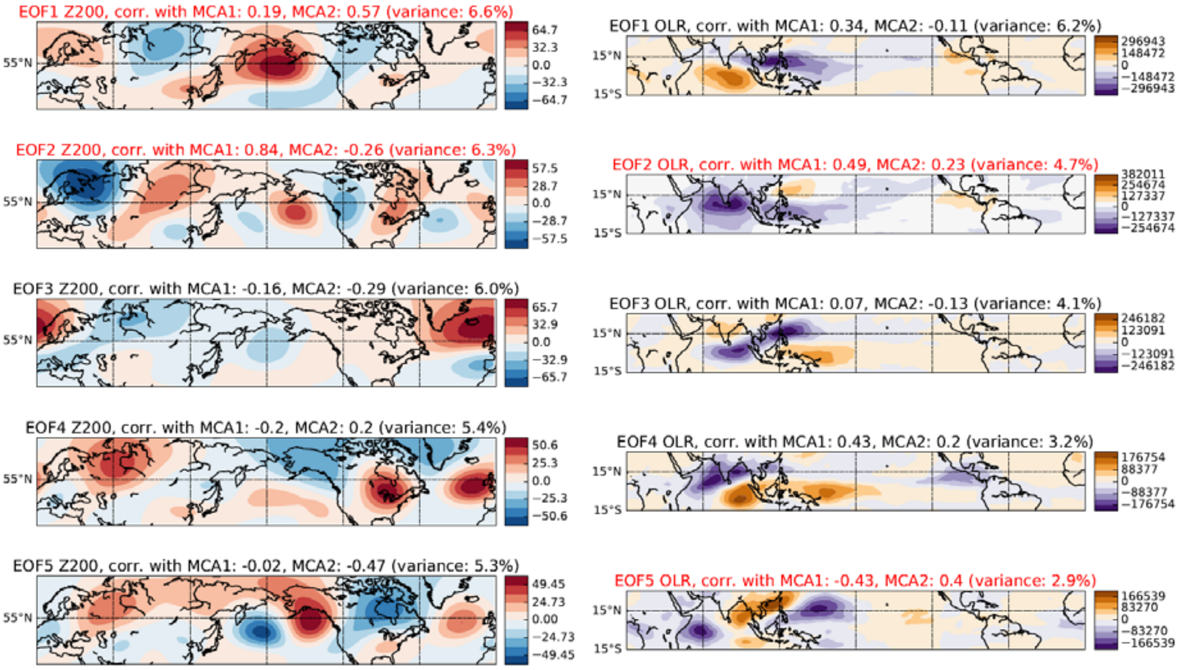

Figure S4. EOF analysis. The right column shows the first five EOF patterns for Z200, the left column shows the first five EOF patterns for OLR. In the title of each panel, the spatial correlation values with the MCA patterns reported in Fig. 2 of the main manuscript are shown. Red font highlights those EOFs that exhibit the strongest overall correlation with the MCA patterns discussed in our manuscript.

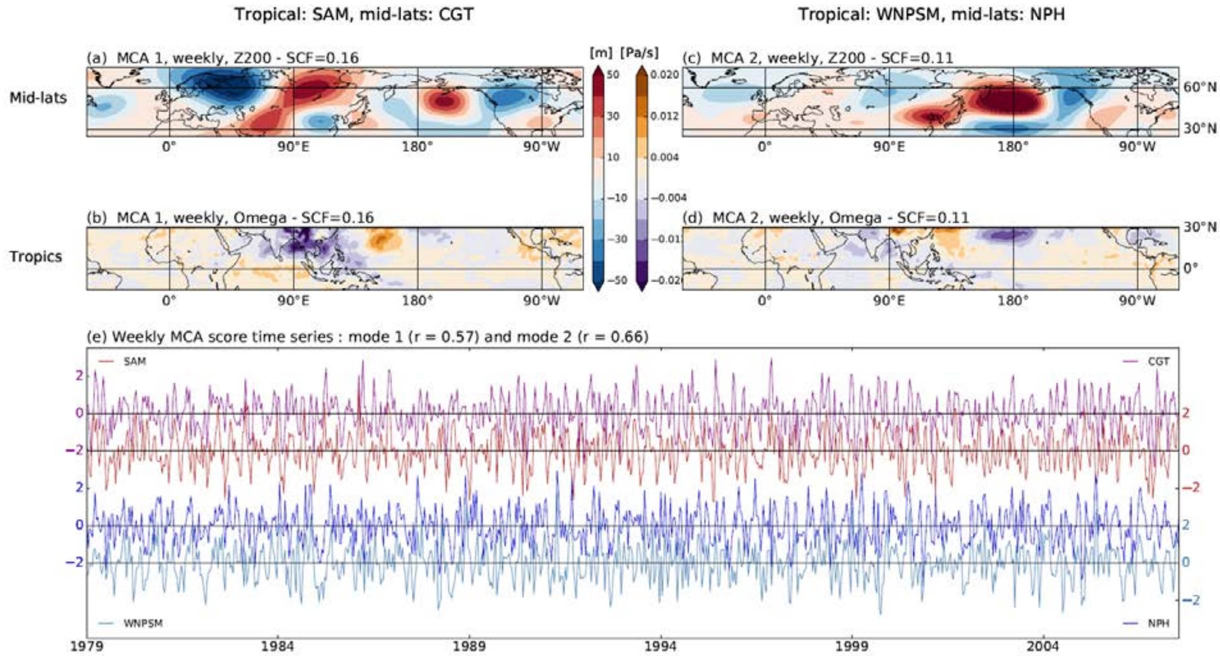

Figure S5. MCA of mid-latitude Z200 and tropical vertical velocity at intraseasonal time-scales. Panels (a) and (b) show the first MCA mode for mid-latitude geopotential height at 300 hPa (Z200, expressed in m) (25-75° N) and tropical vertical velocity (Omega, expressed in Pa/s) (15°S-30°N), respectively, at the weekly time scale. The first MCA highlights the circumglobal teleconnection (CGT) pattern in the mid-latitudes and the South Asian monsoon (SAM) in the tropical belt. Panels (c) and (d): Same as for panel (a) and (b) but for the second MCA mode. This mode depicts the North Pacific High (NPH) in the mid-latitudes and the western North Pacific summer monsoon (WNPSM) in the tropical belt. The squared covariance fraction (SCF) of each MCA mode is given on top of the panels. Panel (e) shows the time series of MCA scores for the two MCA modes at the weekly time-scale. Each MCA pattern has its own time series, i.e. one for tropical OLR and one for mid-latitude Z200 (note that different *y*-axes are used).

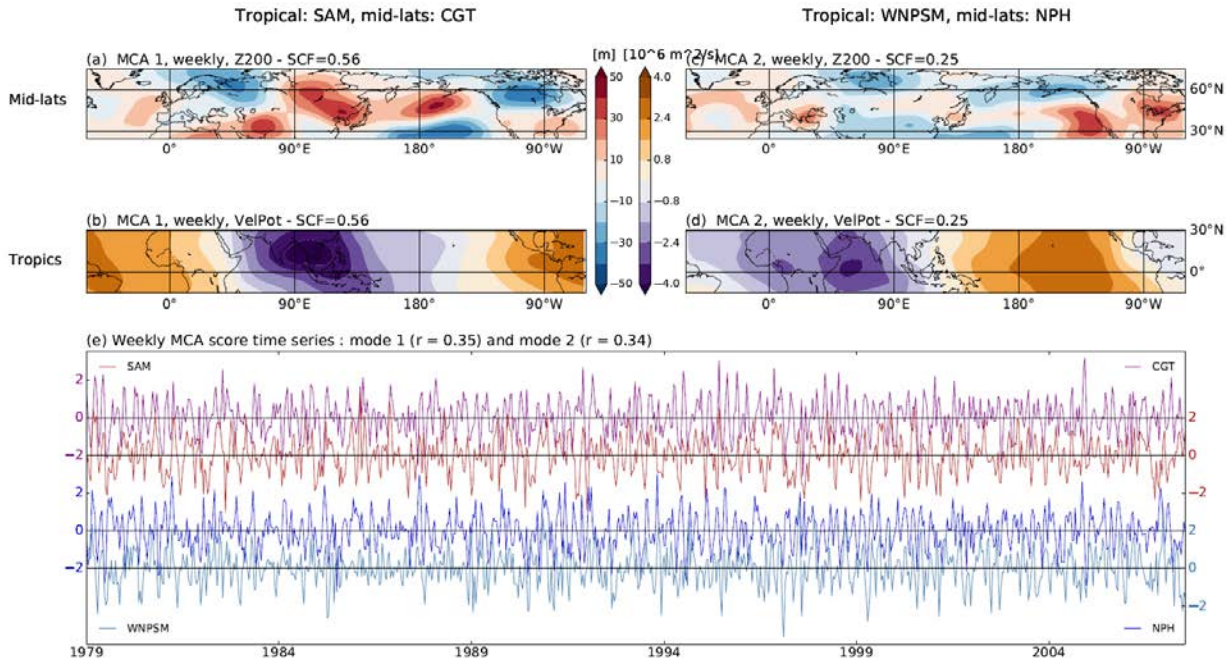

Figure S6. MCA of mid-latitude Z200 and tropical velocity potential at intraseasonal time-scales. Panels (a) and (b) show the first MCA mode for mid-latitude geopotential height at 300 hPa (Z200, expressed in m) (25-75° N) and tropical velocity potential (VelPot, expressed in m^2/s) (15°S-30°N) respectively, at the weekly time scale. The first MCA highlights the circumglobal teleconnection (CGT) pattern in the mid-latitudes and the South Asian monsoon (SAM) in the tropical belt. Panels (c) and (d): Same as for panel (a) and (b) but for the second MCA mode. This mode depicts the North Pacific High (NPH) in the mid-latitudes and the western North Pacific summer monsoon (WNPSM) in the tropical belt. The squared covariance fraction (SCF) of each MCA mode is given on top of the panels. Panel (e) shows the time series of MCA scores for the two MCA modes at the weekly time scale. Each MCA pattern has its own time series, i.e. one for tropical OLR and one for mid-latitude Z200 (note that different *y*-axes are used).

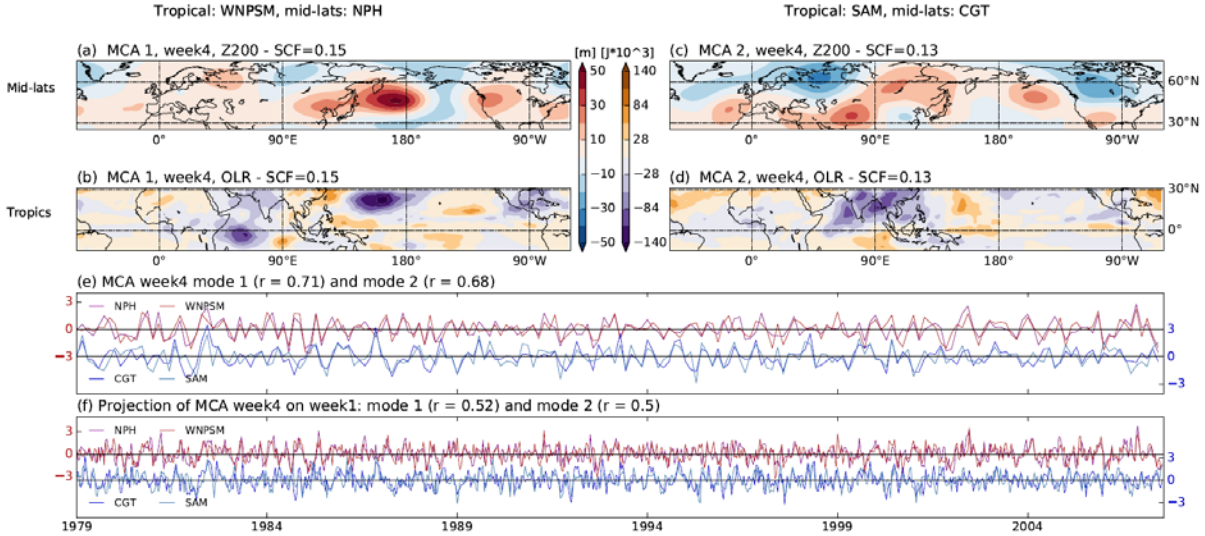

Figure S7. MCA of mid-latitude Z200 and tropical OLR at intraseasonal time scales. Panels (a) and (b) show the first MCA mode for mid-latitude Z200 (25-75° N) and tropical OLR (15°S-30°N), respectively, at the 4-weekly time scale. This mode depicts the North Pacific high (NPH) in the mid-latitudes and the western North Pacific summer monsoon (WNPSM) in the tropical belt. Panels (c) and (d): Same as for panel (a) and (b) but for the second MCA mode. The second MCA highlights the circumglobal teleconnection (CGT) pattern in the mid-latitudes and the South Asian monsoon (SAM) in the tropical belt. The squared covariance fraction (SCF) of each MCA mode is given on top of the panels. Panel (e) shows the time series of MCA scores for the two MCA modes at 4-weekly time scale. Each MCA pattern has its own time series, i.e. one for tropical OLR and one for mid-latitude Z200 (note that different *y*-axes are used). Panel (f): Same as panel (e) but for weekly time series obtained by projecting the 4-weekly MCA modes on weekly OLR and Z200 3D fields.

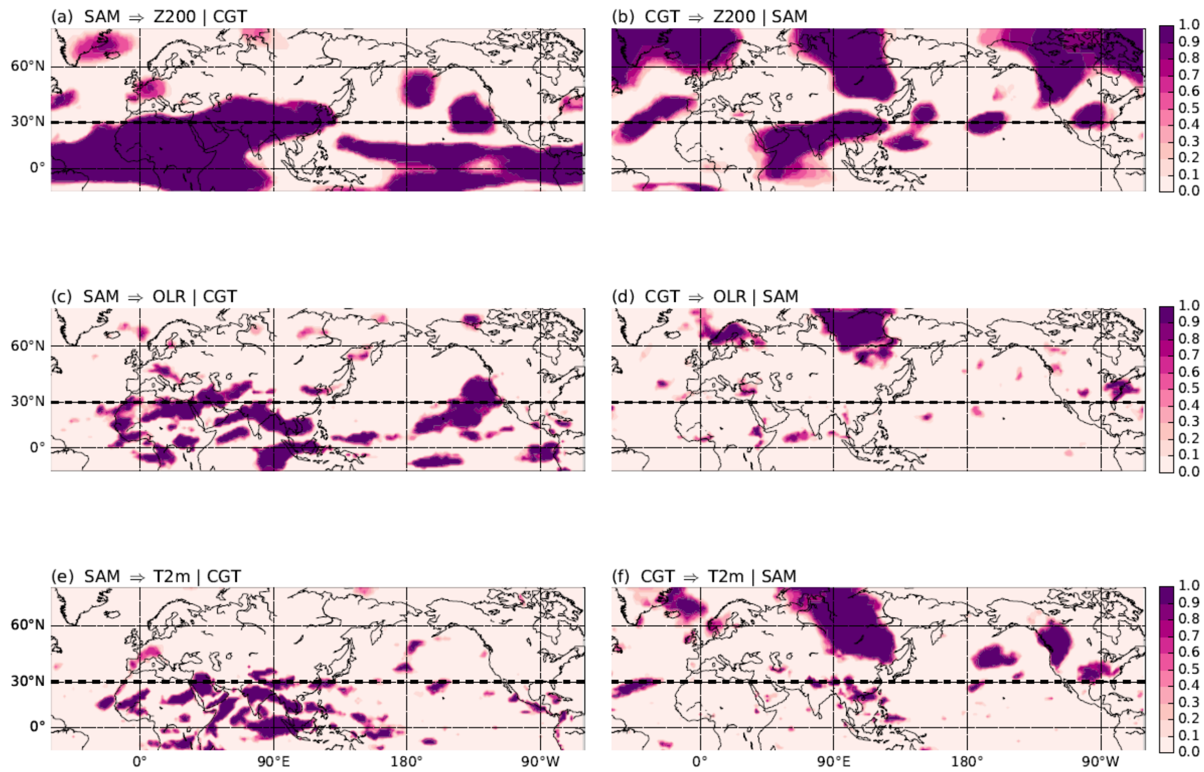

Figure S8. Robustness test for causal maps as shown in Fig. 3 of the main manuscript. Dark purple shows regions that show a significant causal link at a significance level of alpha $\alpha = 0.05$ (after applying the false discovery rate correction) in all ten causal maps obtained by iteratively removing a set of 4 consecutive years each time, with a value of 1 meaning that a region is always identified.

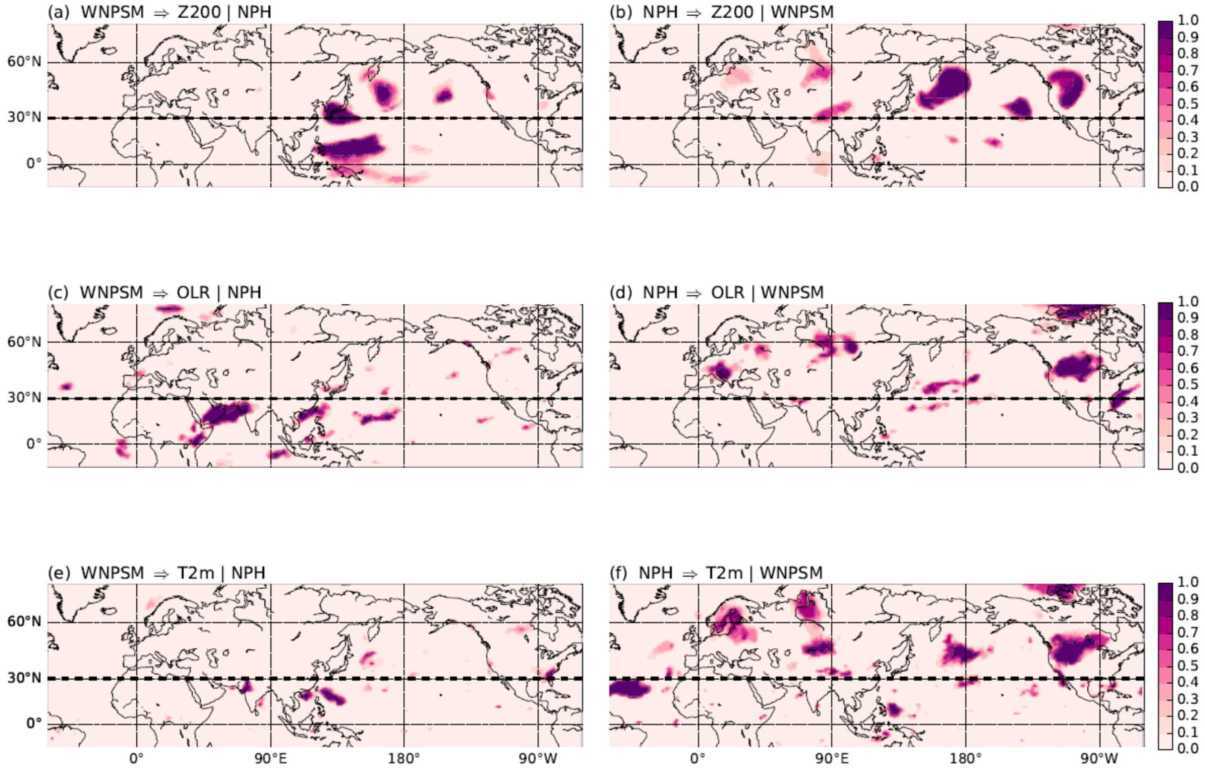

Figure S9 Robustness test for causal maps as shown in Fig. 4 of the main manuscript. Dark purple shows regions featuring a significant causal link at a significance level of alpha $\alpha = 0.05$ (after applying the false discovery rate correction) in all the causal maps obtained by iteratively removing a set of 4 consecutive years each time, with a value of 1 meaning that a region is always identified.

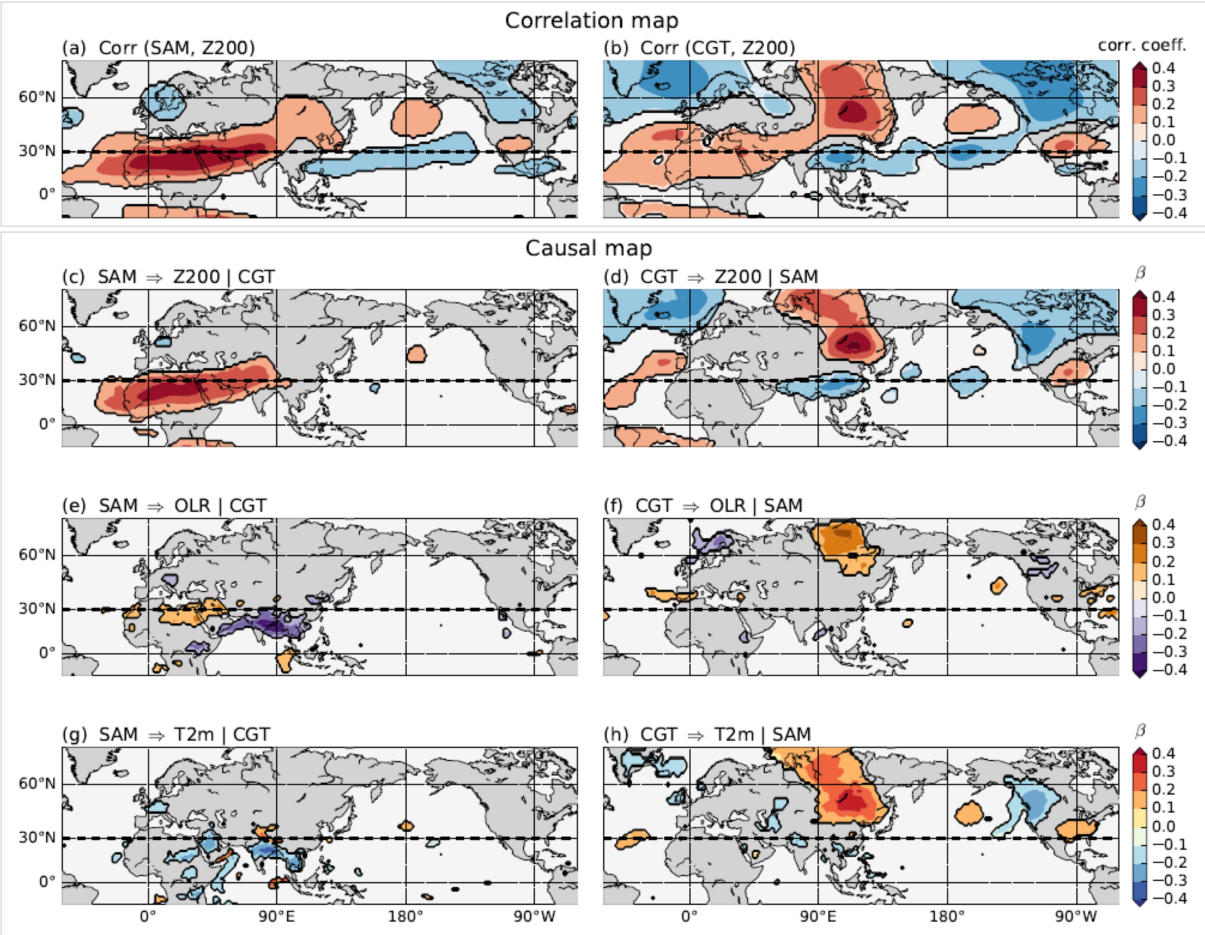

Figure S10. Influence of MCA mode 2 on Northern Hemisphere circulation. Panel (a): correlation map between the weekly SAM time series (obtained from 4-weekly MCA modes, see SI Fig. S1) and the Z200 field. Panel (b): Same as panel (a) but for the correlation between weekly CGT time series and the Z200 field. Panel (c): path coefficient β for link $SAM_{\tau=-1} \rightarrow Z200_{\tau=0}$ for a 3-actor CEN built with SAM, CGT and Z200. Panel (d): Same as panel (c) but for the link $CGT_{\tau=-1} \rightarrow Z200_{\tau=0}$. Panels (e) and (g): Same as panel (c) but for the influence of SAM on OLR and T2m fields respectively. Panels (f) and (h): Same as panel (d) but for the influence of CGT on OLR and T2m fields respectively. Only path coefficients β with $p < 0.05$ (accounting for the effect of serial correlations) are shown by black contours, while grid points which are found significant only with non-corrected p-values are shaded. The dashed black line located at 30°N shows the border between the tropical and the mid-latitude belt.

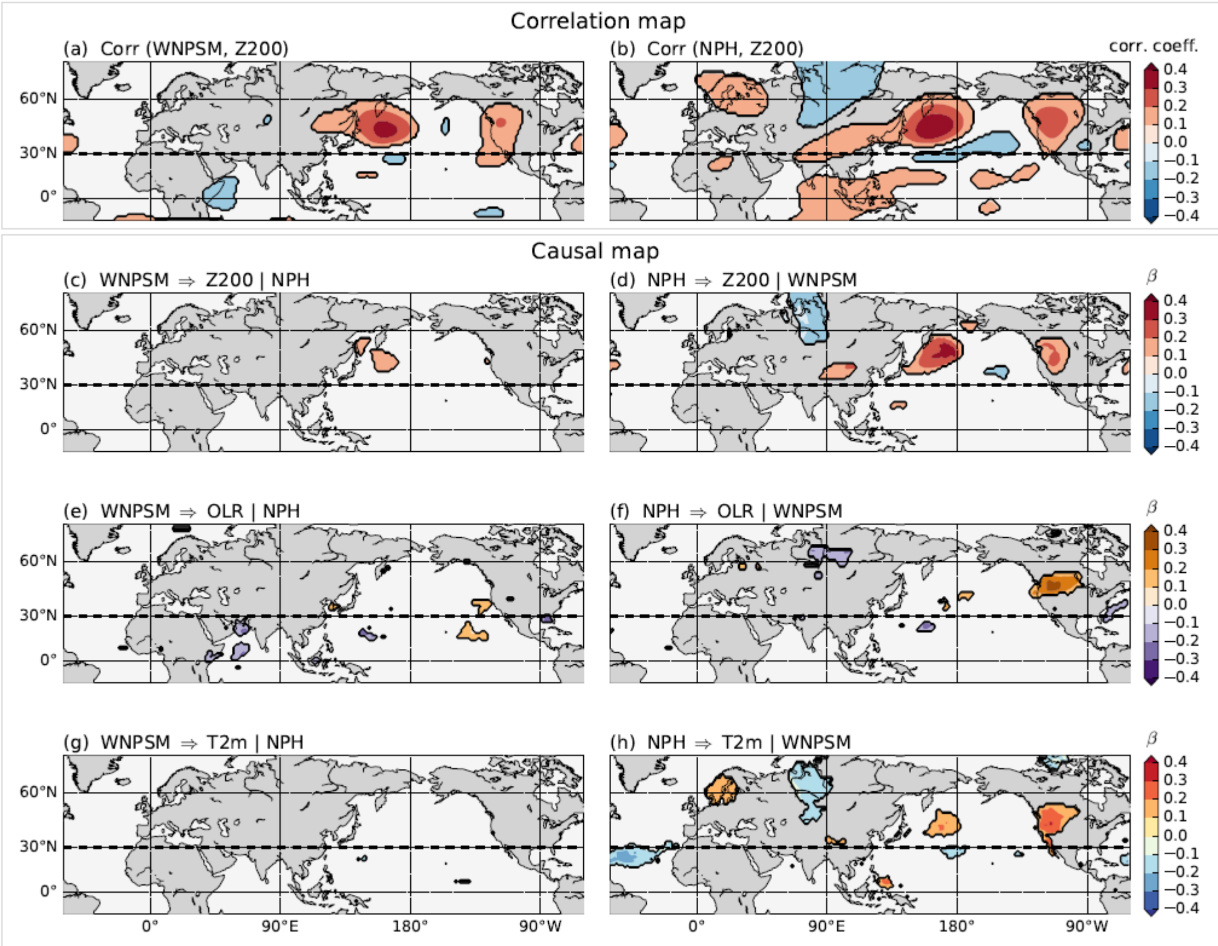

Figure S11. Influence of MCA mode 1 on Northern Hemisphere circulation. Panel (a): correlation between the weekly WNPSM time series (obtained from 4-weekly MCA modes, see SI Fig. S1) and the Z200 field. Panel (b): As panel (a) but for the correlation between weekly NPH time series and the Z200 field. Panel (c): path coefficient β for the link WNPSM $_{\tau=-1}$ → Z200$_{\tau=0}$ in a 3-actors CEN built with WNPSM, NPH and Z200. Panel (d): Same as panel (c) but for the link NPH $_{\tau=-1}$ → Z200$_{\tau=0}$. Panels (e) and (g): Same as panel (c) but for the influence of WNPSM on OLR and T2m fields respectively. Panels (f) and (h): Same as panel (d) but for the influence of NPH on OLR and T2m fields respectively. Only path coefficients β with $p < 0.05$ (accounting for the effect of serial correlations) are shown by black contours, while grid points which are found significant only with non-corrected p-values are shaded. The dashed black line located at 30°N shows the border between the tropical and the mid-latitude belt.

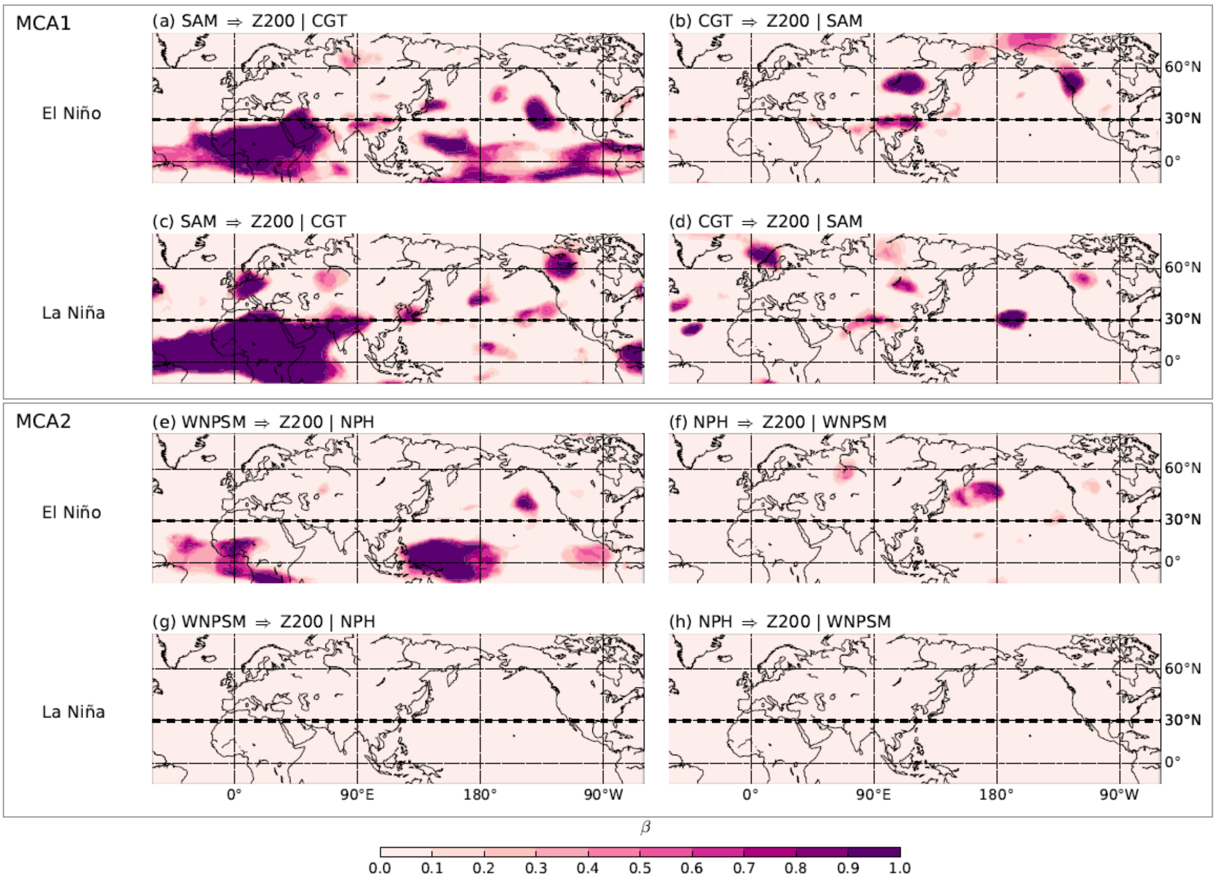

Figure S12. Robustness test for causal maps as shown in Fig. 5 of the main manuscript. Dark purple shows regions featuring a significant causal link at a significance level of alpha $\alpha = 0.05$ (after applying the false discovery rate correction) in all ten causal maps obtained by iteratively removing a set of 4 consecutive years each time, with a value of 1 meaning that a region is always identified.

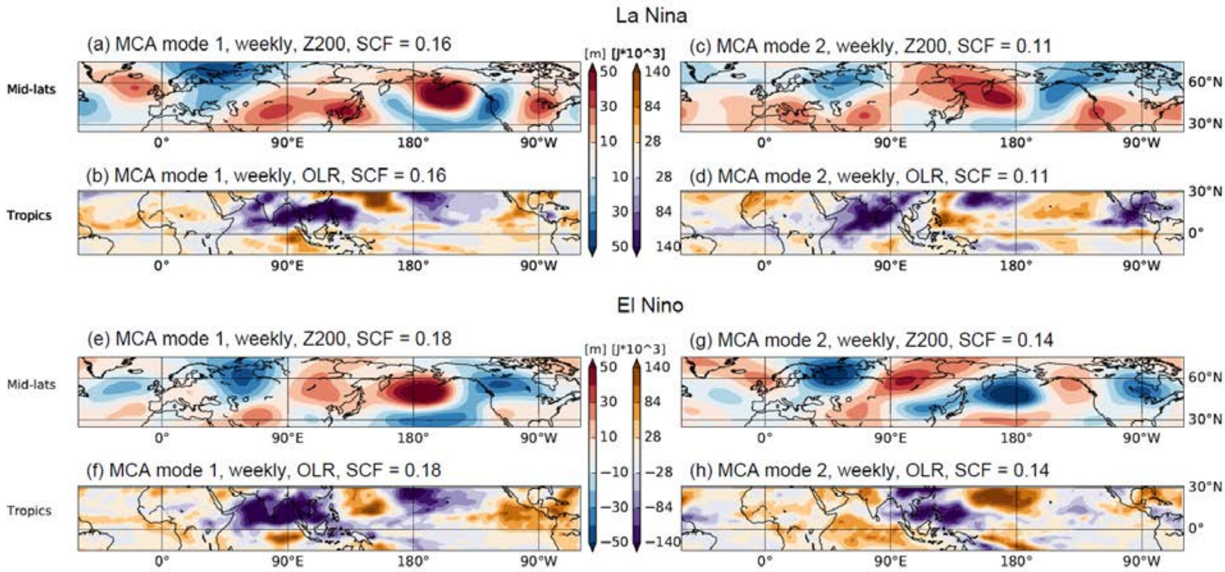

Figure S13. MCA modes during different ENSO phases. Panels (a) and (b) show the first MCA mode for mid-latitude Z200 (25-75° N) and tropical OLR (15°S-30°N), respectively, at the weekly time scale and during La Niña years only. Panels (c) and (d): Same as for panel (a) and (b) but for the second MCA mode. Panels (e) to (h): Same as panels (a) to (d) but for El Niño summers.

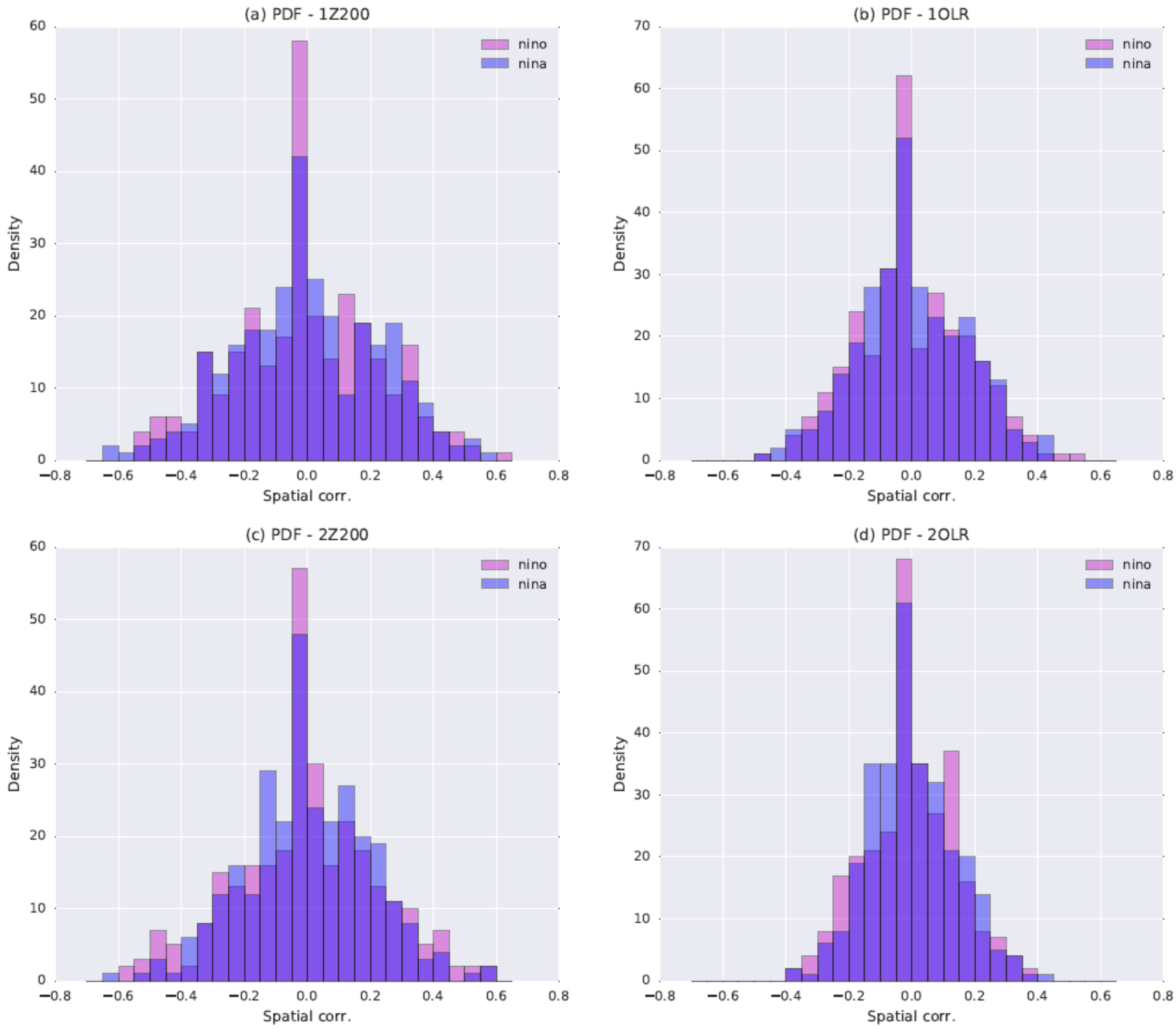

Figure S14. Histograms for spatial correlation between each weekly MCA mode and the Z200/OLR fields. Panel (a): histogram for the spatial correlation between the weekly MCA mode 1 Z200 pattern and the Z200 weekly field. Panel (b): Same as panel (a) but for the weekly MCA mode 1 OLR pattern and the weekly OLR fields. Panel (c): Same as panel (a) but for MCA mode 2. Panel (d): Same as panel (b) but for MCA mode 2.

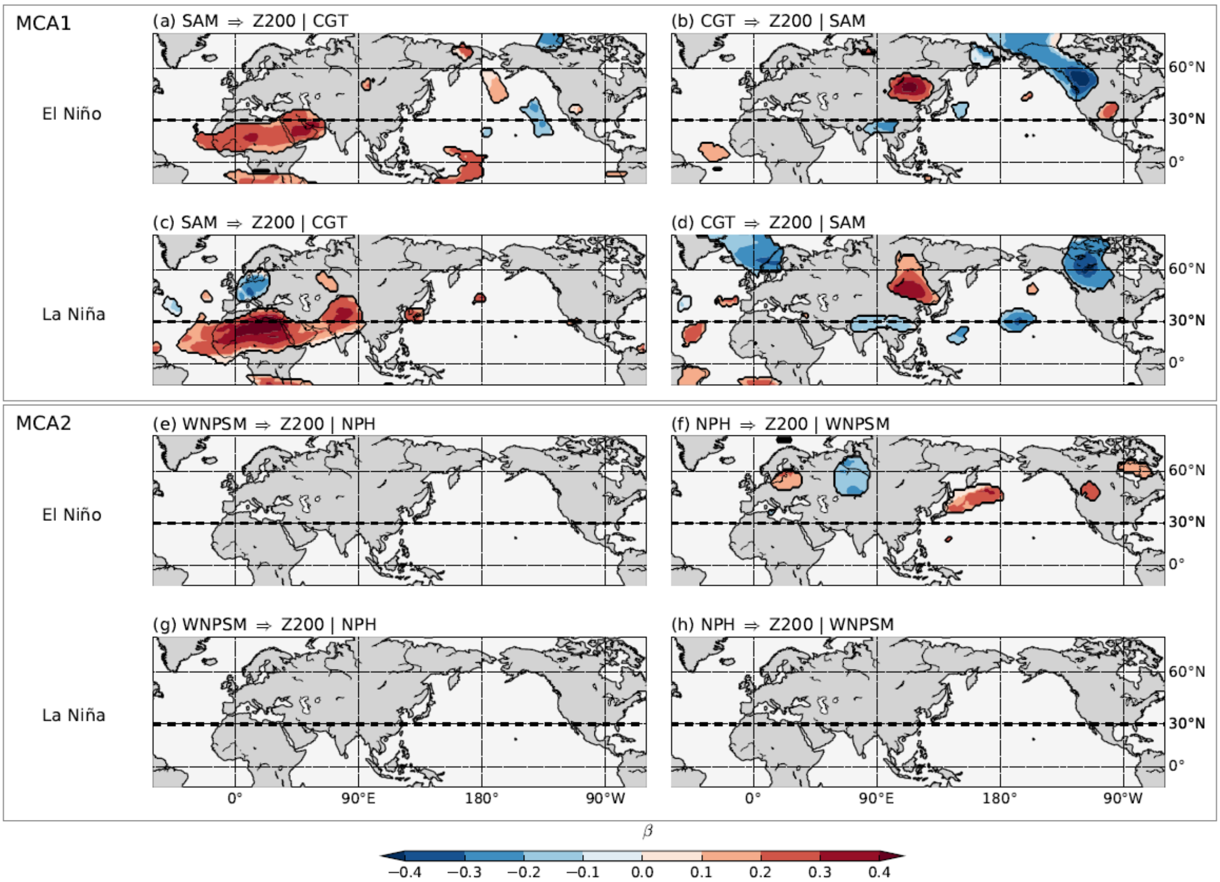

Figure S15. Causal maps: ENSO influence. Panel (a) shows the β values for the link WNPSM $_{\tau=-1} \rightarrow$ Z200$_{\tau=0}$ a 3-actor CEN built with WNPSM, NPH and Z200 during El Niño years. Panel (b): Same as panel (a) but for La Niña years. Panels (c) and (d): Same as panels (a) and (b) but for the link NPH $_{\tau=-1} \rightarrow$ Z200$_{\tau=0}$. Panels (e) and (f): Same as panels (a) and (b) but for the link SAM $_{\tau=-1} \rightarrow$ Z200$_{\tau=0}$ from a 3-actors CEN built with SAM, CGT and Z200. Panels (g) and (h): Same as panels (e) and (f) but for the link CGT $_{\tau=-1} \rightarrow$ Z200$_{\tau=0}$. Only β values with $p <$ 0.05 are shown.

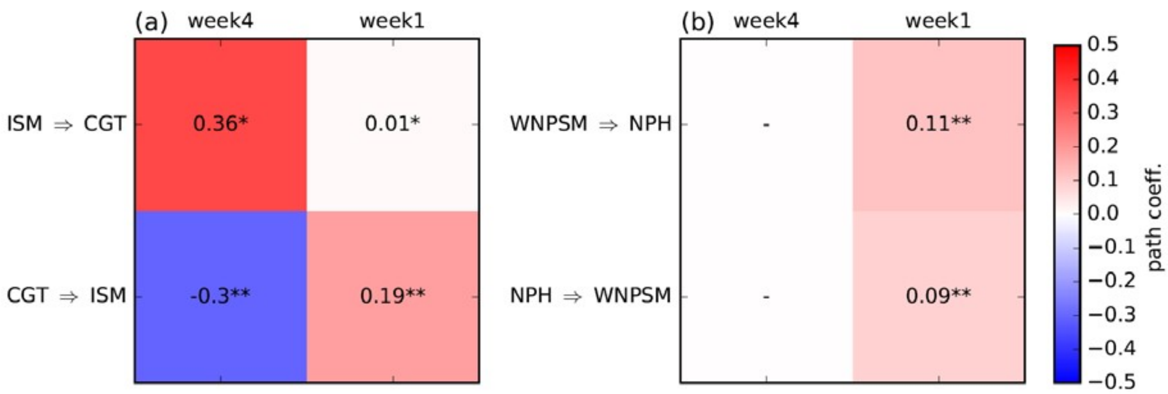

Figure S16. Same as Figure 2 but for time series obtained from OLR and Z200 fields having removed 4-weekly variability.

El Niño	**La Niña**
1979	1983
1982	1984
1986	1985
1987	1988
1991	1995
1994	1998
1997	1999
2002	2000
2004	2005
2006	2007
2009	2008
2014	2010
2015	2011
	2017

Table S1. Classification of El Niño and La Niña years. See Method section in the main text for the description of the classification used.